

Domain wall induced modulation of low field H-T phase diagram in patterned superconductor-ferromagnet stripes

Ekta Bhatia,¹ Abhishek Talapatra,² Jyoti Ranjan Mohanty,² Zoe H. Barber,³ Ilari J. Maasilta,⁴ and Kartik Senapati^{1, a)}

¹⁾*School of Physical Sciences, National Institute of Science Education and Research (NISER), HBNI, Bhubaneswar, Odisha, India-752050*

²⁾*Department of Physics, Indian Institute of Technology Hyderabad, Hyderabad 502285, India*

³⁾*Department of Materials Science and Metallurgy, University of Cambridge, 27 Charles Babbage Road, CB3 0FS, UK*

⁴⁾*Nanoscience Center, Department of Physics, University of Jyväskylä, P. O. Box 35, FI-40014, Jyväskylä, Finland*

(Dated: 10 January 2019)

We present a systematic study of the magnetic domain wall induced modulation of superconducting transition temperature (T_c) in Nb/Ni bilayer stripes. By varying the thickness of the Ni layer from 20 nm to 100 nm we have been able to measure the low field T_c -H phase diagram spanning the Néel domain wall and Bloch domain wall range of thicknesses. Micromagnetic simulations and magnetic force microscopy measurements confirmed a stronger out-of-plane stray field in the Bloch domain walls compared to the Néel walls. A suppression in T_c was observed in the magnetization reversal region of the Ni film, the magnitude of which followed linearly to the strength of the out-of-plane stray field due to the domain walls. The magnitude of the stray field was quantified by comparing the T_c of the suppressed region of H- T_c phase diagrams with the unaffected part of the H- T_c curve. With Bloch domain walls a change in T_c of more than 60 mK was observed which is much more compared to the earlier reports. We believe that the narrow stripe geometry of the bilayers and the transverse external field maximized the effect of the domain walls in the Ni layer on the overlying superconducting film, leading to a larger change in T_c . This observation may be useful for domain wall controlled switching devices in superconducting spintronics.

PACS numbers: 74.62.-c, 75.60.Ch, 74.45.+c

^{a)}Kartik Senapati: kartik@niser.ac.in

The field of superconducting spintronics has attracted wide research interest in recent years^{1,2}. One of the reasons is the additional spin degree of freedom provided by the Cooper pairs to the spintronic devices. Since such devices inevitably contain co-functioning S and F components, new interesting phenomena such as π -phase superconductivity³, spin-triplet supercurrent⁴, odd-frequency pairing⁵ and long-range magnetic proximity effects⁶ emerge out of the natural competition between superconducting and ferromagnetic orders. These effects have been well studied in a variety of devices over the past years⁷⁻¹⁰. In the context of superconducting spintronics, the effect of magnetization dynamics of ferromagnetic components on the superconducting components is also a very pertinent question. Typically, magnetization reversal of one or more ferromagnetic components is the key functional aspect of spintronic devices. During the magnetization reversal process, the domain walls in ferromagnets produce stray fields which can alter the properties of a proximal superconducting layer and, therefore, may affect the overall device properties. Prior experimental observations of the superconducting spin switch effect¹¹, domain wall superconductivity^{12,13} and triplet superconductivity⁴ are qualitatively consistent with theoretical predictions of F/S

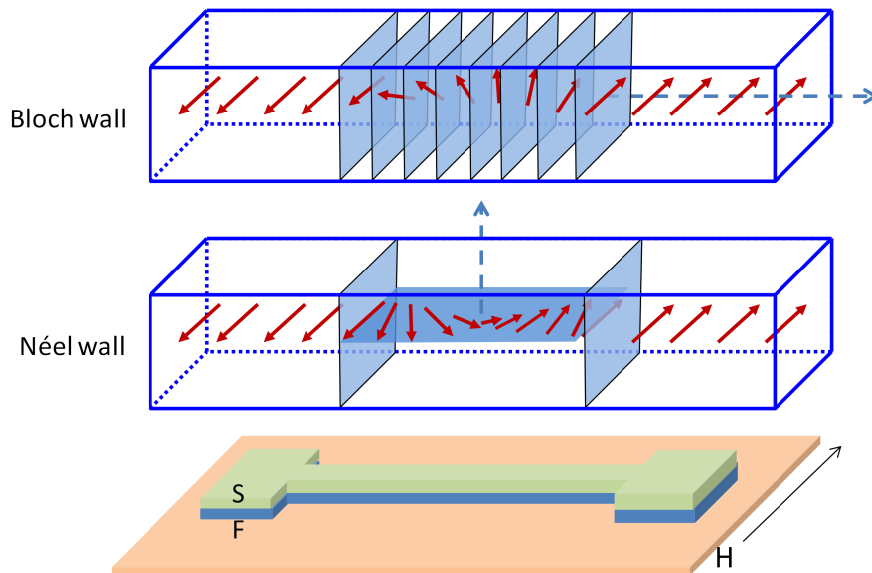


FIG. 1. Schematic view of magnetization rotation in a Néel wall and Bloch wall between two domains in a stripe geometry. The dashed arrows show the axis of rotation of magnetization. An overlying superconducting layer, as shown here in the S-F bilayer stripe geometry, would directly sense the out-of-plane stray field of the walls.

proximity effects involving non-uniform ferromagnets^{14,15}. Stray fields invariably accompany inhomogeneous magnetization distributions such as domain walls and sample edges. They can suppress superconductivity by the classical orbital effect or by dissipative vortex motion. Thus, a definitive comparison between theory and experiment in superconducting spintronics is problematic without considering the exact strength of stray field. Therefore, it is an important parameter to know in proximity effect based or domain state dominated superconducting spintronic devices^{16,17}. However, no direct quantification of the extent to which a superconducting layer is affected by these stray fields, are available in the literature. Some earlier reports have, however, measured the stray field of magnetic thin films using electro-optic studies¹⁸, photo-emission electron microscopy¹⁹, magnetic force microscope (MFM)²⁰, quantitative MFM²¹, and magnetic transmission X-ray microscopy²².

In superconducting-spintronics devices, the domain structure and hence the stray field of domain walls may be modified below the superconducting transition temperature. In such embedded magnetic layers, there is no direct way of quantifying the stray magnetic field. However, the effects of such stray fields on various superconducting multilayer structures have been explored in the literature. Steiner et al.²³ studied the role of stray fields in an exchange-biased system of the type Fe/Nb/Co/CoO and in Fe/Nb bilayers. Hu et al.²⁴ reported the stray field and the superconducting surface spin valve effect in La_{0.7}Ca_{0.3}MnO₃/YBa₂Cu₃O_{7- δ} bilayers. Yang et al.²⁵ have reported the modulation of superconductivity by the stray field of Bloch walls in Nb/Y₃Fe₅O₁₂ hybrids. In this context, we have quantified the stray field of Néel domain walls and Bloch domain walls of nickel films in Nb/Ni bilayer stripes below the superconducting transition temperature. For this purpose, we have carefully measured the resistive transition temperatures of lithographically patterned narrow channels of Nb/Ni bilayers, as a function of an in-plane applied magnetic field. We observed a systematic variation of suppression in the low field T_c of Nb/Ni stripes as a function of the thickness of the underlying Ni layer. The observed suppression of T_c gives a direct measure of the strength of domain wall stray field, using the standard BCS type H-T phase diagram. The strength of the out-of-plane stray field of Bloch domain walls was found to be much larger compared to Néel domain walls in the buried nickel film, below the superconducting transition.

A series of Nb-Ni bilayer thin films was prepared at room temperature in a vacuum chamber with base pressure in the range of 10⁻⁹ mbar, using dc-magnetron sputtering of high

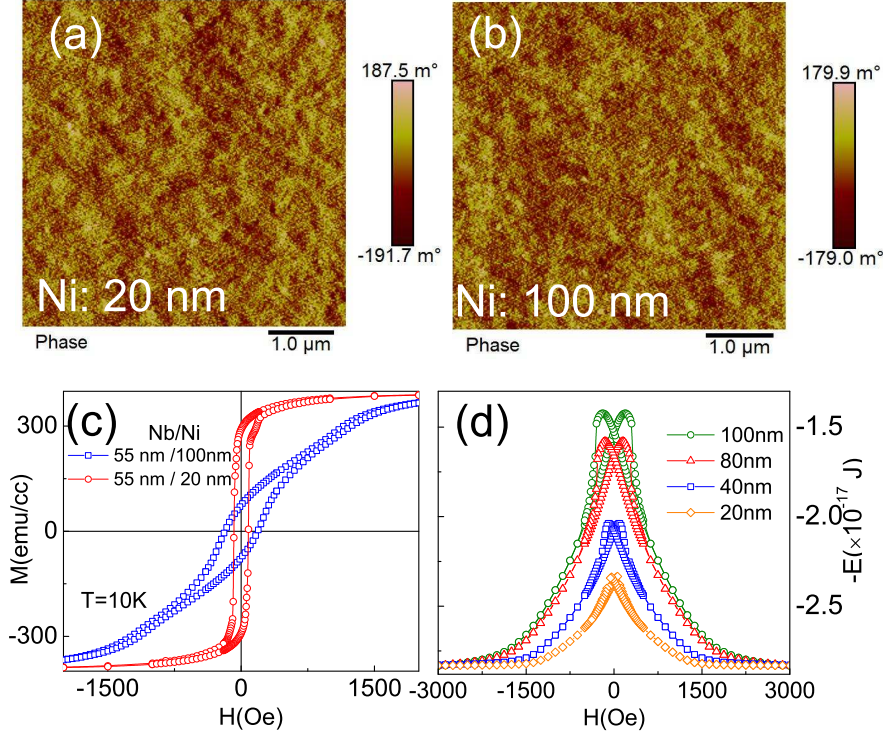


FIG. 2. Remnant state MFM images showing magnetic phase contrast of nickel films of (a) 20 nm (b) 100 nm thickness. Images were taken in the remnant state after saturating the samples in presence of 6000 Oe in-plane magnetic field. (c) Magnetic hysteresis loops of Nb/Ni bilayer with nickel film thickness of 20 nm and 100 nm at a temperature of 10 K. (d) Negative of demagnetization energy, extracted from micro-magnetic OOMMF simulation, is plotted as a function of an in-plane magnetic field for nickel films. This quantity is a measure of the strength of domain wall stray field of the material, which maximizes at coercive field.

purity(99.999%) niobium and nickel targets on cleaned Si-SiO₂ substrates. The thickness of the bottom nickel layer was varied from 20 nm to 100 nm with steps of 20 nm, while the thickness of the top niobium layer was kept fixed at 55 nm ± 5 nm in all cases. Films were then patterned into narrow stripes of width 3 micron using a combination of electron beam lithography, reactive ion etching and chemical etching techniques. Transition temperatures were found by electrical transport measurements performed in a standard four probe geometry. Superconducting transition temperatures were measured in the presence of an in-plane applied magnetic field along the width of the stripe. For each measurement, the films were saturated by applying a field of 4000 Oe and then ramped to the measurement field value at

a temperature of 5K. Magnetization measurements were performed in a SQUID magnetometer with magnetic field applied parallel to the plane of the films. MFM measurements of Ni films were performed in the remnant state of the films after magnetizing with an in-plane field of 6000 Oe.

Fig.1 shows the typical magnetization rotation configuration of domain walls in the Bloch and Néel wall regimes. In an S-F bilayer stripe geometry, the superconducting film in the long striped region of the pattern would be maximally affected by the out of plane stray fields of the domain walls in the underlying ferromagnetic film. Depending on the film thickness, any ferromagnetic film may have Néel domain walls or Bloch domain walls as shown in Fig.1. Typically, the domain wall energy per unit area (the sum of anisotropy, exchange and stray field energy densities) gradually decreases with increasing film thickness for Bloch walls, whereas for Néel walls the domain wall energy increases with increasing film thickness. Therefore, below a certain threshold value of film thickness (where the Néel wall and Bloch wall energy densities match), Néel walls become energetically favorable, whereas at a higher thickness, Bloch walls are preferred energetically²⁶⁻²⁸. It has been predicted theoretically that the crossover thickness in nickel films is about 50 nm^{29,30}. These domain walls have a different out of plane component of the stray field as shown in Fig.1.

Fig.2(a), 2(b) and 2(c) shows the MFM images and MH loop of nickel films with 20nm and 100 nm thickness. These MFM images have been taken in the remnant state of the samples, after saturating them in an in-plane field of 6000 Oe. Therefore, the MFM images correspond to the remnant moment of the Ni films. Measurements were taken at a fixed lift height of the magnetic tip (at 60 nm) from the surface to increase the probability of visualizing domain walls pinned into the topographic defects. We observe that the magnetic contrast of both 20 nm and 100 nm Ni films are roughly the same, whereas one would expect more magnetic contrast in the case of the 100 nm film which is expected to have more out-of-plane stray field due to the Bloch walls. This apparent contradiction is, however, possible to explain if we notice the remnant magnetic moments of corresponding films in the magnetization loops in Fig.2(c). Clearly, the remnant moment of the 100 nm film is almost 4 times lower than the remnant moment of the 20 nm film. Hence, the magnetic contrast in the MFM image of the 100 nm nickel film should be four times weaker in comparison to the 20 nm nickel film, as the MFM images were taken in the remnant state. Therefore, similar magnetic contrast observed in MFM images of these two samples indicates that the effective out of

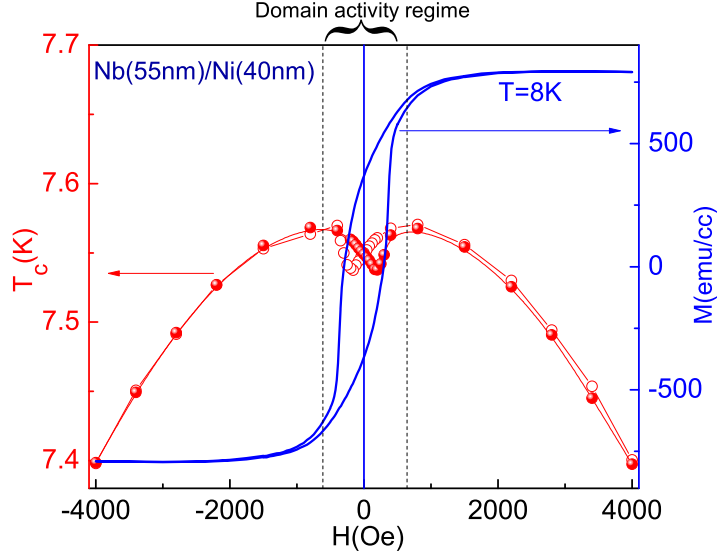


FIG. 3. Transition temperature is shown as a function of in-plane applied magnetic field swept in forward and backward directions, for Nb(55nm)/Ni(40nm) bilayer stripe. Right hand side axis shows the corresponding magnetization loop of the Nb/Ni bilayer at a temperature of 8 K. The minima of the T_c curves clearly match with the coercive field of the Ni layer.

plane component of the 100 nm nickel film is four times more than that of the 20 nm nickel film. This suggests that the domain walls for the 20 nm nickel film are of Néel type and the domain walls for the 100 nm nickel film are of Bloch type. This result is in agreement with the previous literature^{29,30}.

To further check the out-of-plane stray field component as a function of thickness of the magnetic layer, we have performed 3D micro-magnetic simulations³¹ on Nickel films. For these simulations, the x and y dimensions of the samples were kept fixed as 2 μm and 1 μm , respectively. The z dimension was varied from 20 nm to 100 nm for different samples. Here, x axis refers to the direction along the length of stripes, y axis refers to the direction along the width of the stripes and z axis refers to the axis transverse to the sample plane. The cell size for simulation was kept as (10, 10, 10) nm in (x, y, z) directions. Magnetic field was directed along the width (y axis) of the stripe in the plane of the film. The values of saturation moment, anisotropy constant, and the exchange constant for the simulations

of magnetization in Ni films were taken from the literature^{32,33}. In Fig.2(d), we plot the negative of the demagnetization energy (E) obtained from the simulations, normalized with the thickness. In magnetic materials, negative of the demagnetization energy is directly proportional to the domain wall stray field³⁴. From Fig.2(d), it is clear that the 100 nm Ni film has a much stronger out-of-plane stray field (which maximizes at the coercive field) compared to the thinner films.

After establishing the existence a larger out-of-plane stray field in the Bloch thickness range, in Fig.3 we show the T_c - H phase diagram for a patterned Nb/Ni bilayer(55nm/40nm) along with the magnetic hysteresis curve of the same bilayer. While ramping the magnetic field down from the saturation field, domain activity starts at around the field value at which the hysteresis loop opens up, as shown by the dotted lines in Fig.3. A decrease in transition temperature with decreasing magnetic field was observed for the Nb/Ni stripes, in the range of magnetic domain activity in the Ni layer. In fact, the low-field T_c was found to follow the magnetic hysteresis loop, attaining a minimum value at a field roughly matching with the coercive field of the nickel layer. On increasing the magnetic field in the opposite direction, from zero, T_c again recovered to the normal value. During the magnetization reversal process, the out of plane stray field of domain walls locally affects superconductivity along the stripe^{12,35,36}, resulting in the observed decrease in superconducting transition temperature. This decrease was maximum at the coercive field, because near the coercive field one would expect the maximum domain wall density, producing a large stray field. In the saturated state, the Ni film behaves as a single domain with minimum domain wall stray field.

In order to emphasize the change in T_c , Fig.4(a) shows the normalized R-T curves at three different fields for the bilayer with 100 nm thick Ni film. T_c has been defined as the temperature at 50% of the normal state resistance. Clearly, the transition at -300 Oe, which is close to the coercive field of the Ni layer in this bilayer, is lower by ~ 64 mK compared to the transitions at fields of 1572 Oe and -1572 Oe. In Fig.4(b), we show a comparison of the T_c - H phase diagrams of patterned Nb/Ni bilayer stripes with nickel layer thicknesses of 20nm, 40nm, 80nm, and 100nm. We notice that the effect of domain wall stray field, near the low magnetic field region, is minimal in the case of 20 nm thick Ni film, which has Néel domain walls. This effect indicates a weaker out-of-plane component of the domain wall stray field, as expected for the Néel walls. We also observe that in the saturation field range the T_c - H curves are BCS-like, in all cases. The suppression of T_c in the domain activity

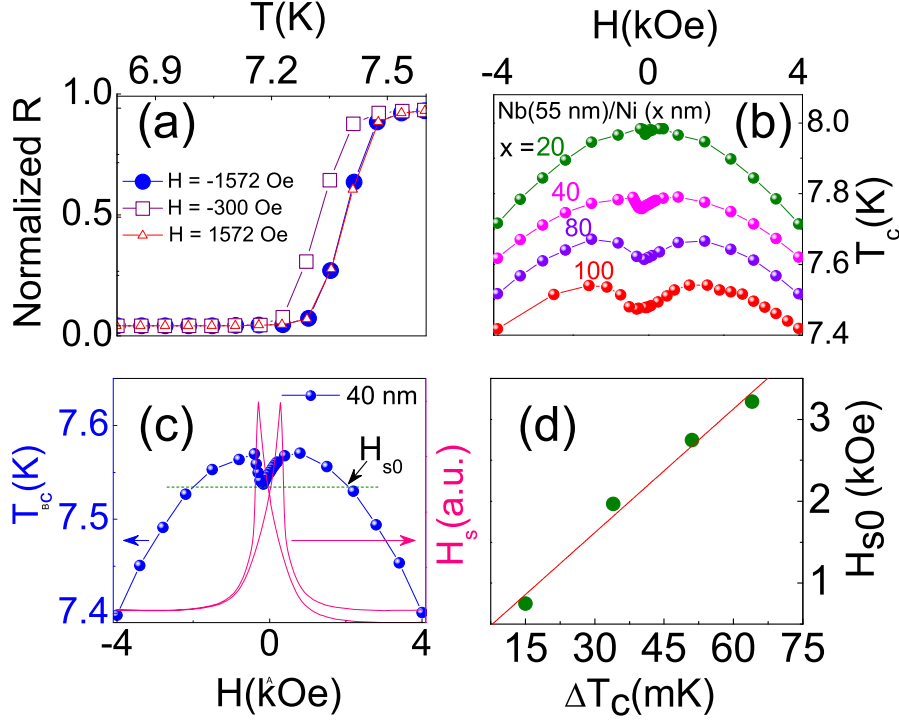


FIG. 4. (a) Normalized resistance vs temperature curves in magnetic fields near the coercive field and saturation field for the Nb/Ni bilayer with 100 nm Ni layer. (b) Comparison of H-T phase diagram of Nb(55)/Ni(x) bilayer stripes with Ni film thickness(x) of 20nm, 40nm, 80nm, and 100nm. (c) H-T diagram of the Nb/Ni bilayer stripes with 40 nm Ni is plotted (on the left hand axis) along with the stray field (H_s , on the right hand axis) calculated from the measured magnetization loop, following Patino et al.³⁷ as described in the text. The dotted line shows the convention used for extracting maximum effective out-of-plane stray field (H_{s0}) from the H-T diagram of all samples. (d) H_{s0} is compared with the maximum change observed in T_c from T_c -H phase diagrams (panel b) of Nb(55)/Ni(x) bilayer stripes.

regime of T_c -H phase diagram can only be due to the stray field generated by the domain walls, in addition to the small external field. On the other hand, the suppression of T_c at higher fields (in the saturation range of Ni films) is due to the external applied field as expected. Since the number of domains and the corresponding domain walls in the FM film follow the magnetic hysteresis loop, the average stray field is a function of applied magnetic field. In the saturation field range, the domain wall stray field becomes negligible and in the coercive field range it becomes maximum. Following Patiño et al.³⁷, the field dependence of H_s can be extracted from the magnetization loop as

$$H_s(H_{ap}) = H_{s_0}(1 - |M(H_{ap})/M_s|)$$

where H_{s_0} , M and M_s are the maximum stray field at coercive field, the magnetization, and the saturation magnetization, respectively. In Fig 4(c) we have plotted the calculated stray field using this formalism, in order to emphasize the fact that domain wall stray field is the origin of the suppression of T_c in the low field regime. We have estimated the maximum strength of the stray field by drawing a horizontal line at the minimum T_c . The field value where this horizontal line crosses the H-T phase diagram in the higher field range was taken as the effective maximum out-of-plane stray field (H_{s_0}). The extracted H_{s_0} is plotted with the change in T_c near the coercive field (ΔT_c) in Fig 4(d). A stray field strength of more than 3000 Oe was observed for the bilayer with 100nm Ni and ~ 700 Oe for bilayer with 20 nm Ni. Stray field value of 400 Oe has been reported earlier for asymmetric Neel walls in a magnetically patterned $\text{Ir}_{17}\text{Mn}_{83}/\text{Co}_{70}\text{Fe}_{30}$ exchange bias layer system²¹. However, the present estimates are much more direct estimates of the stray field strength compared to earlier reports. The fact that the overall ΔT_c scales linearly with H_{s_0} indicates that H_{s_0} is a true measure of the average local field strength due to the domain walls. Thus, by tuning the domain walls and switching them either on or off via external magnetic field, superconductivity in the overlying Nb film can be effectively modulated.

In summary, we have studied patterned Nb/Ni bilayer stripes with different thicknesses of nickel layer spanning the range from Néel domain walls to Bloch domain walls. Low field T_c -H phase diagrams of these patterned structures were found to follow the magnetization loop of the underlying Ni layer. In the domain activity region, a reduction in T_c was observed which maximized near the coercive field of the Ni film. This indicated that the observed suppression in T_c is a result of the domain wall induced stray field of the underlying Ni layer. We were able to extract and compare the maximum strength of stray field due to the Néel domain walls and Bloch domain walls using the superconducting transition of the overlying Nb layer. The overall reduction in T_c was found to be much smaller in the case of Néel domain walls compared to the Bloch domain walls. The relative strength of the out-of-plane stray field due to Néel domain wall and Bloch domain wall of a plain nickel film was also examined using magnetic force microscopy and micro-magnetic simulations. The variation of stray field with thickness was consistent in both the cases. There is no simpler way of estimating the local magnetic field of the domain walls in an embedded superconductor-ferromagnet hybrid below the superconducting transition. Our method gave

a direct measure of the local stray field emanating from the domain walls, which is a very pertinent parameter for performance optimization of superconducting spintronics devices. Furthermore, the observed change in T_c of more than 60 mK with Bloch walls is much more than earlier reports. This large magnitude of domain wall induced tuning of T_c may be useful for domain wall controlled switching components in superconducting spintronics.

We acknowledge the funding from National Institute of Science Education and Research(NISER), DST-Nanomission (SR/NM/NS-1183/2013) and DST SERB (EMR/2016/005518) of Govt. of India.

REFERENCES

- ¹J. Linder and J. W. A. Robinson, Nat. Phys. **11**, 307 (2015).
- ²J. Linder and K. Halterman, Phys. Rev. B **90**, 104502 (2014).
- ³V. V. Ryazanov, V. A. Oboznov, A. Yu. Rusanov, A. V. Veretennikov, A. A. Golubov and J. Aarts, Phys. Rev. Lett. **86**, 2427 (2001).
- ⁴T. S. Khaire, M. A. Khasawneh, W. P. Pratt and N. O. Birge, Phys. Rev. Lett. **104**, 137002 (2010).
- ⁵F. S. Bergeret, A. F. Volkov and K. B. Efetov, Rev. Mod. Phys. **77**, 1321 (2005).
- ⁶I. V. Bobkova and A. M. Bobkov, Phys. Rev. Lett. **108**, 197002 (2012).
- ⁷F. S. Bergeret, A. F. Volkov, and K. B. Efetov, Phys. Rev. Lett. **86**, 4096 (2001).
- ⁸J. W. A. Robinson, G. B. Halasz, A. I. Buzdin, and M. G. Blamire, Phys. Rev. Lett. **104**, 207001 (2010).
- ⁹J. W. A. Robinson, J. D. S. Witt, and M. G. Blamire, Science **329**, 59 (2010).
- ¹⁰R. S. Keizer, S. T. B. Goennenwein, T. M. Klapwijk, G. X. Miao, G. Xiao, and A. Gupta, Nature (London) **439**, 825 (2006).
- ¹¹J. Y. Gu, C.-Y. You, J. S. Jiang, J. Pearson, Ya.B. Bazaliy, and S. D. Bader, Phys. Rev. Lett. **89**, 267001 (2002).
- ¹²Z. Yang, M. Lange, A. Volodin, R. Szymczak, and V. V. Moshchalkov, Nature Mater. **3**, 793 (2004).
- ¹³A. Yu. Rusanov, M. Hesselberth, J. Aarts, and A. I. Buzdin, Phys. Rev. Lett. **93**, 057002 (2004).
- ¹⁴A. I. Buzdin, A. V. Vedyayev, and N.V. Ryzhanova, Europhys. Lett. **48**, 686 (1999).
- ¹⁵S. Oh, D. Youm, and M. R. Beasley, Appl. Phys. Lett. **71**, 2376 (1997).
- ¹⁶J. Zhu, X. Cheng, C. Boone, and I. N. Krivorotov, Phys. Rev. Lett. **103**, 027004 (2009).
- ¹⁷M. Flokstra and J. Aarts, Phys. Rev. B **80**, 144513 (2009).

- ¹⁸Ch. Schwink and O. Scharpf, *Phys. Status Solidi* **30**, 637 (1968).
- ¹⁹A. Krasnyuk, S. A. Nepijko, A. Oelsner, C. M. Schneider, H. J. Elmers, and G. Schonhense, *Appl. Phys. A* **88**, 793 (2007).
- ²⁰M. Barthelmess, C. Pels, A. Thieme, and G. Meier, *J. Appl. Phys.* **95**, 5641 (2004).
- ²¹N. Zingsem, F. Ahrend, S. Vock, D. Gottlob, I. Krug, H. Doganay, D. Holzinger, V. Neu, and A. Ehresmann, *J. Phys. D: Appl. Phys.* **50**(49), 495006 (2017).
- ²²G. Meier, R. Eiselt, M. Bolte, M. Barthelme β , T. Eimüller, and P. Fischer, *Appl. Phys. Lett.* **85**, 1193 (2004).
- ²³R. Steiner and P. Ziemann, *Phys. Rev. B* **74**, 094504 (2006).
- ²⁴T. Hu, H. Xiao, C. Visani, J. Santamaria and C. C. Almasan, *New J. Phys.* **13**, 033040 (2011).
- ²⁵Z. Yang and V. V. Moshchalkov, *J. Appl. Phys.* **109**, 083908 (2011).
- ²⁶L. Néel, *C.R. Acad. Sci. (Paris)* **241**, 533 (1955).
- ²⁷F. Bloch, *Z. Phys.* **74**, 295335 (1932).
- ²⁸S. Middelhoek, *J. Appl. Phys.* **34**, 1054 (1963).
- ²⁹A. Aharoni, *Introduction to the theory of ferromagnetism* (Oxford University Press, Oxford, 2000).
- ³⁰C. T. Hsieh, J. Q. Liu and J. T. Lue, *Appl. Surf. Sci.* **252**, 1899-1909 (2005).
- ³¹M. Donahue and D. Porter, *Interagency Report NISTIR 6376*, National Institute of Standards and Technology, Gaithersburg, Maryland (1999).
- ³²P. R. Boardman, *Computer simulation studies of magnetic nanostructures*, Ph.D. thesis, University of Southampton, November 2006.
- ³³S. L. Whittenburg, N. Dao, and C. A. Ross, *Physica B* **306**, 44 (2001).
- ³⁴J. Stöhr, and H. C. Siegmann, *Magnetism: From Fundamentals to Nanoscale Dynamics* (Springer, 2006).
- ³⁵A. Y. Aladyshkin, A. V. Silhanek, W. Gillijns, and V. V. Moshchalkov, *Supercond. Sci. Technol.* **22**, 053001 (2009).
- ³⁶L. Zhigang, W. Wang, L. Zhang, Y. Zhaorong, T. Mingliang and Z. Yuheng, *Scientific Reports* **5**, 18601 (2015).
- ³⁷E. J. Patiño, C. Bell, and M. G. Blamire, *Eur. Phys. J. B* **68**, 73 (2009).